Effects of Convectively Generated Gravity Waves and Rotation on the Organization of Convection

CHANGHAI LIU AND MITCHELL W. MONCRIEFF

National Center for Atmospheric Research, Boulder, Colorado*

(Manuscript received 27 March 2003, in final form 18 March 2004)

ABSTRACT

The effects of latent heating, gravity waves, and planetary rotation on numerically simulated convective cloud systems are investigated. First, the nonlinear response of an initially motionless, uniformly stratified, dry atmosphere to steady heating that interacts with the environment through inertial–gravity waves is examined. Planetary rotation confines the subsidence-induced adiabatic warming to the neighborhood of the heated region on a time scale comparable to the lifetime of mesoscale convective systems. In a moist atmosphere, rotation-induced localized descent stabilizes and dries the near environment and decreases the convective available potential energy. The Tropics is therefore a preferred region for convective clustering.

This hypothesis is tested in two sets of multiday convection-resolving simulations on f planes representative of the Tropics, subtropics, and midlatitudes. Convection is maintained by radiative cooling and surface fluxes of heat and moisture. In a motionless mean state, convective clustering is most prominent in the Tropics. In constant easterly flow, tropical convection organizes on three scales. Eastward-propagating convectively coupled gravity waves generate large-scale envelopes of cloudiness. Embedded within these envelopes are westward-traveling mesoscale convective systems that, in turn, contain westward-traveling deep convective cores.

1. Introduction

Latent heat release by precipitating convection has long been recognized as an important energy source for the large-scale circulation of the atmosphere (Riehl and Malkus 1958). Although latent heating is fundamentally of microphysical origin, its distribution is strongly affected by the organization of convection on mesoscales. Gravity waves generated by latent heating feed back to affect convective organization. This macrophysical property is implicit in the approach used by the Tropical Rainfall Measuring Mission (TRMM) to estimate precipitation from space using radar and microwave radiometer measurements. The retrieval algorithms used are based either on observational data (Kummerow et al. 2001) or on synthetic data from cloud-resolving models (Tao et al. 2001). Our objective is to quantify macrophysical aspects using convection-resolving numerical models. In particular, we examine the role of gravity waves and the vertical distribution of heating (convective and stratiform) on convective organization.

Warming of the environment has previously been studied in terms of a response of a stably stratified fluid to localized heating (Bretherton 1987, 1988; Bretherton and Smolarkiewicz 1989; Nicholls et al. 1991; Pandya et al. 1993; Mapes 1993, 1998). The upward transport of mass by convection is compensated by subsidence that warms and dries the environment: the basis of cumulus parameterization of the mass-flux kind. Gravity waves affect the convective available potential energy (CAPE) and the convective inhibition, an aspect examined by Lane and Reeder (2001) in cloud-resolving simulations. This process was suggested to be responsible for the gregarious behavior of tropical convection by Mapes (1993). Subsidence wave fronts associated with the gravest mode make the near field particularly unfavorable to new convection. On the other hand, the heating associated with mesoscale convective systems (MCSs) may excite waves that result in upward displacement at low levels, promoting new convection.

The effect of planetary rotation (the Coriolis acceleration) confines the compensating subsidence to a finite distance, measured by the Rossby radius of deformation, from a heat source, as illustrated by hydrostatic linear theory (Bretherton 1987, 1988). This localization affects low-level lifting and the initiation of nearby convection. We shall quantify the effects of rotation on time scales of many hours using specified convective heating profiles. The rotation-induced modulation of subsidence warming and drying, which occurs on a time scale comparable to typical life cycles of MCSs, will be shown

* The National Center for Atmospheric Research is sponsored by the National Science Foundation.

Corresponding author address: Dr. Changhai Liu, National Center for Atmospheric Research, P. O. Box 3000, Boulder, CO 80307-3000. E-mail: chliu@ucar.edu

strong enough to affect the distribution, scale, and organization of convection, as a function of latitude.

In the following section we summarize the modeling methodology. In section 3 we present numerically simulated nonlinear responses of a uniformly stratified dry atmosphere to thermal forcing that idealizes the latent heating by convective systems. Rotation-induced localization of subsidence warming is quantified and the implications in a moist atmosphere described. Multiday simulations of cloud systems on f planes are presented in section 4. Finally, a summary and discussion follow in section 5.

2. Methodology

We use the two-dimensional Eulerian version of the three-dimensional nonhydrostatic Eulerian/semi-Lagrangian anelastic model of Smolarkiewicz and Margolin (1997). The computational domain is 6000 km wide and 25 km deep with a 2-km horizontal and 0.25-km vertical grid lengths. Free-slip boundary conditions are employed at the rigid boundaries at the top and bottom with fixed conditions at the lateral boundaries of the computational domain. A Rayleigh absorber is applied to the uppermost 5 km and to the 200-km-wide neighborhood of the lateral boundaries of the domain in order to dampen unrealistic reflection of gravity waves.

As in the majority of previous studies on convectively generated gravity waves, the convection is represented by an externally imposed heat source (e.g., Bretherton 1988; Nicholls et al. 1991; Mapes 1993; Pandya et al. 1993). The thermal forcing is localized, time invariant, and slab symmetric. The heating is located in the middle of the model domain and decreases to zero over a specified distance. (The vertical profile of heating is the sum of a deep positive-definite mode of wavelength twice the depth of the heat source and a full-sine mode.) The deep mode mimics the latent heating in the vigorous convective region of an MCS and, by representing lower-tropospheric cooling and upper-tropospheric warming, the shallow mode models the stratiform region of an MCS. Appropriate combinations of these profiles idealize the latent heating distributions in various cloud-cluster regimes. Specifically, the heating distribution is

$$Q(x, z) = Q_0 \cos\left(\frac{\pi x}{2L}\right)\left[\sin\left(\frac{\pi z}{H}\right) - \gamma \sin\left(\frac{2\pi z}{H}\right)\right],$$
$$|x| \le L; \qquad 0 \le z \le H, \tag{1}$$

where Q_0 is the amplitude of the heating rate and L and H are the half-width and depth of the heat source, respectively. Values of $Q_0 = 0.01$ K s^{-1}, $L = 15$ km, and $H = 12$ km are used.

The parameter γ defines the relative contribution from the stratiform-like heating. Four values (0, 1/4, 1/2, and 3/4) were selected to test sensitivity to the vertical distribution of heating. Figure 1 shows profiles through the center of the heat sources. The value $\gamma = 0$ represents convective cloud systems without a stratiform region. The larger γ is, the greater the stratiform contribution. Three of the four cases correspond to positive-definite heating. We concentrate on $\gamma = 1/2$ (dotted curve in Fig. 1) and comment briefly on the other cases.

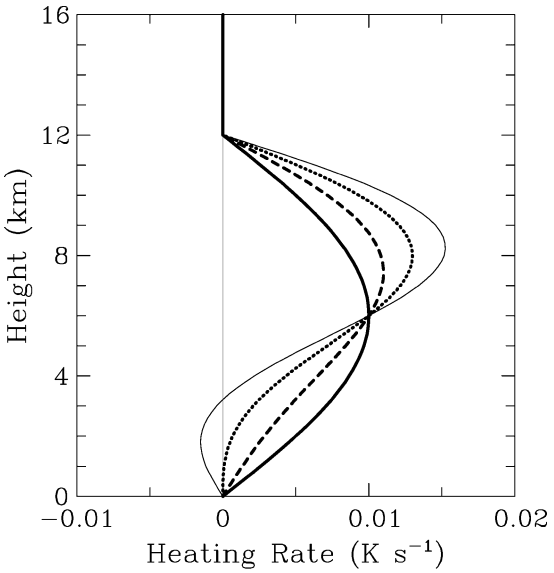

FIG. 1. Vertical heating profiles at the center of the heat sources. The thick solid, dashed, dotted, and thin solid lines correspond to γ = 0, 1/4, 1/2, and 3/4 in Eq. (1), respectively.

It should be pointed out that several additional mechanisms as well as convective heating have been proposed for the gravity wave excitation within the cloud. The first mechanism refers to the mechanical forcing of transient oscillating updrafts within a convective system (Clark et al. 1986; Fovell et al. 1992): oscillatory updrafts impinge upon an overlying stable layer (e.g., the tropopause), impulsively deform the isentropes, and produce vertically propagating gravity waves. The second mechanism refers to the obstacle effect of cumulus clouds due to differential environmental flows relative to the cloud. Cumulonimbus convection in shear may act as an obstruction to horizontal air motion, exciting gravity waves. Finally, Lane et al. (2001) demonstrated that the nonlinear advections by the cloud's own circulation contribute significantly to the gravity wave generation. Although diabatic heating alone may not accurately represent the source of gravity waves within a convective system, the aforementioned processes are responsible mainly for high-frequency, upward propagating waves. Consequently, the resultant environmental modifications integrated in the vertical would be insignificant because the effects of high-frequency modes are averaged out as indicated in Lane and Reeder (2001). In other words, the use of an external heating to characterize the source appears to be an adequate simplifi-

cation because the gravity-wave-induced modulation on the environmental thermodynamics is the focus.

3. Dry simulations

We conducted eight numerical experiments, each corresponding to one of the four profiles with or without planetary rotation. The model is initialized with a motionless stably stratified atmosphere of constant stratification

$$N = \sqrt{\left(\frac{gd\theta}{\theta dz}\right)} = 10^{-2}\ \mathrm{s}^{-1}$$

below 16 km, and $N = 2.6 \times 10^{-2}\ \mathrm{s}^{-1}$ above. Note that the maximum height of the heating (12 km) is below the tropopause. The external heating is switched on at the initial time and subsequently maintained.

In the idealized simulations, the background flow and shear are omitted. Previous studies have identified various ways in which shear affects gravity waves. First, vertical shear influences gravity wave propagation and refracts the phase lines, creating an asymmetry between the upstream and downstream propagating waves. Second, in the presence of tropospheric wind shear, clouds with different heights generate waves at the level of neutral buoyancy with different ground-based frequencies, thus broadening the ground-based frequency spectrum (Lane et al. 2001). Furthermore, under some circumstances wind shear might result in wave absorption at critical levels or cause ducting of gravity waves. Taken together, wind shear could have a substantial effect on the modeling results presented below and will be the subject of future studies.

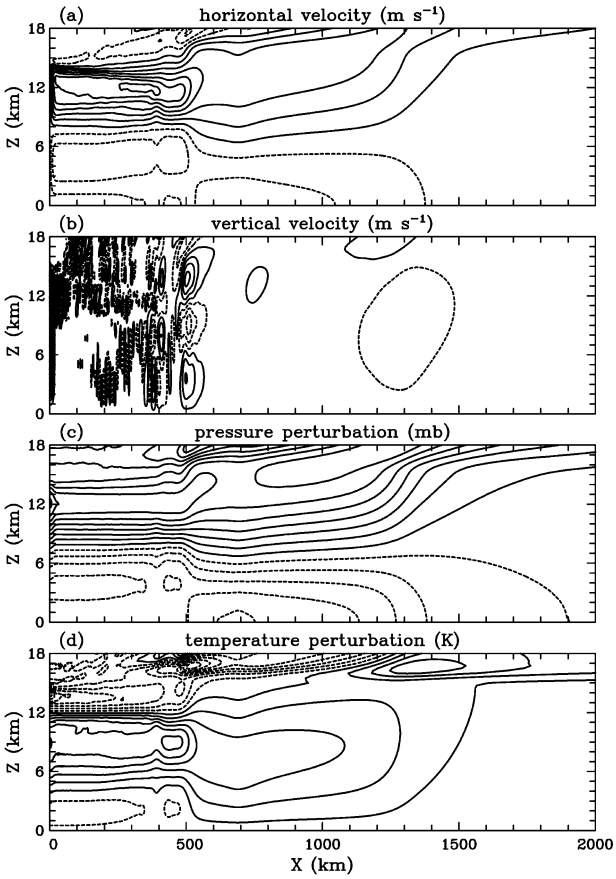

FIG. 2. Simulated fields at 8 h for $f = 0$ and $\gamma = 1/2$. (a) Horizontal wind (contour interval 2 m s^{-1}), (b) vertical velocity (contour interval 0.05 m s^{-1}), (c) perturbation pressure (contour interval 2 mb), and (d) perturbation temperature (contour interval 0.5 K).

a. Planetary rotation omitted

In an initially motionless environment, gravity waves disperse symmetrically; therefore, unless otherwise stated, only half of the computational domain is displayed. Figure 2a shows the characteristic inflow toward the heated region at lower levels and outward flow aloft, a typical mass adjustment to deep, localized thermal forcing. Strong ascent in the heated region (Fig. 2b) causes the adiabatic cooling that counters the imposed heating. The surrounding area is dominated by widespread vertical displacements associated with gravity waves of long wavelengths.

The two gravest wave modes with respect to the depth of the heating have by far the largest amplitude. The fast-propagating wave (phase speed about 45 m s^{-1}) has a half-wavelength roughly equal to the depth of the heat source. The wave front position at $z = 0$ is about $x = 1300$ km. The wave front with a horizontal phase velocity of about 18 m s^{-1} and vertical wavelength comparable to the heating depth is located around $x = 500$ km. The former generates deep, broad subsidence with a midtropospheric maximum, whereas the latter produces comparatively narrower but stronger upward motion in the lower and upper troposphere and middle-level descent. These do not possess a periodic structure in time or horizontal space, distinct to the ordinary monochromatic gravity waves. Qualitatively, the results are similar to those of Nicholls et al. (1991) and Mapes (1993). Note that the amplitude of the vertical motion associated with the slow wave is more than twice that of the fast wave.

If latent heating is confined in a region capped by a rigid lid, classical linear gravity wave theory applied to a motionless base state gives the vertical wavelength and the dispersion equation for nth mode (hydrostatic) gravity waves

$$\lambda_z = \frac{2Z_T}{n} \quad \text{and} \quad c = c_g = \frac{NZ_T}{n\pi}, \tag{2}$$

respectively, where λ_z is the vertical wavelength, c and c_g are the the horizontal phase and group speeds, Z_T is the heating depth, and n is an integer. Hence, the horizontal phase and group speeds are equal and proportional to the Brunt–Väisälä frequency and the vertical wavelength; the longer waves move faster than the

shorter ones, consistent with the modeling results. For the case discussed here, $Z_T = 12$ km and $N = 10^{-2}$ s^{-1}, the calculated phase speeds for the first two modes are approximately 38 and 19 m s^{-1}, respectively. These values are not exactly the same as the respective counterpart in the simulation because the imposed heating does not extend to the tropopause, which itself is not a rigid surface.

Figure 2c shows that the extensive negative (positive) pressure perturbations at lower (upper) levels are dominated by the gravest modes. The horizontal gradient is consistent with the generation of horizontal wind perturbations (Fig. 2a). The temperature field in Fig. 2d exhibits significant warming in the 4–12-km layer, overlying relatively weak cooling and underlying strong cooling in the vicinity of the source. Because the adiabatic cooling associated with upward motion in the forcing region offsets the imposed heating, only moderate midtropospheric warming and weak lower-level cooling occur. For the most part, the two gravest modes account for the temperature perturbations that extend from the source region to the leading front of the slow wave. Shallower, slower moving gravity waves are confined between the source and the slow mode, and their net effects are comparatively insignificant. In particular, the low-level cooling associated with the slow mode overcompensates for the warming associated with the fast mode. The extensive deep warming in the remote environment (beyond the slow-wave front) attributes solely to the adiabatic subsidence around the leading front of the fast wave. The large-amplitude perturbations above 16 km are a consequence of the strong stratification in the stratosphere.

b. *Effect of planetary rotation*

With rotation added, the response is manifested by a spectrum of inertial–gravity wave modes. The corresponding dispersion equation is given by

$$\omega^2 = \frac{k^2N^2 + m^2f^2}{k^2 + m^2}. \tag{3}$$

For hydrostatic waves ($k \ll m$), the dispersion relation can be approximated as

$$\omega^2 = \frac{k^2N^2 + m^2f^2}{m^2}. \tag{4}$$

The horizontal phase and group speeds are

$$c = \sqrt{1 + \frac{m^2f^2}{k^2N^2}}\frac{N}{m} \quad \text{and} \quad c_g = \frac{1}{\sqrt{1 + \frac{m^2f^2}{k^2N^2}}}\frac{N}{m}, \tag{5}$$

respectively. It follows that the inclusion of the earth's rotation increases the horizontal phase speed but decreases the horizontal group velocity by the factor

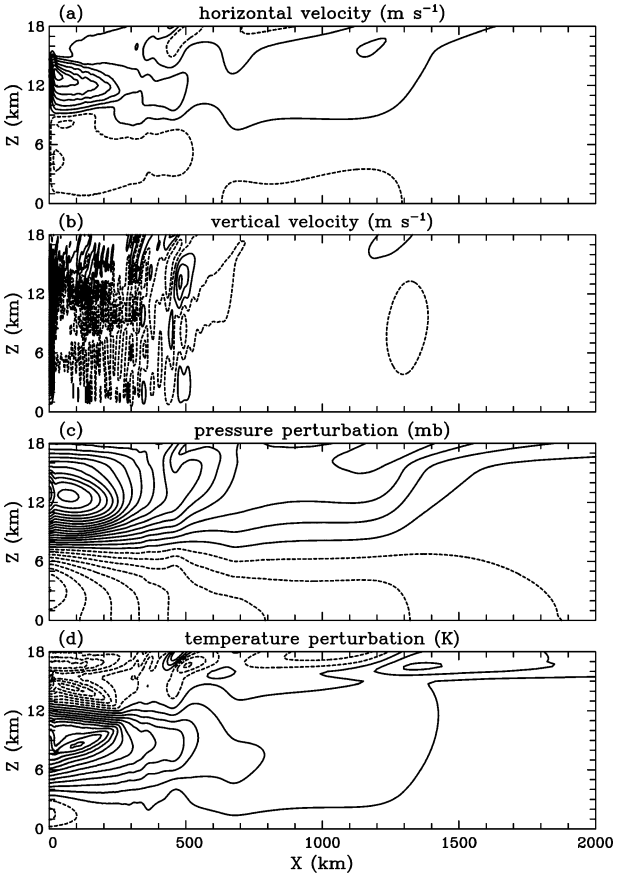

FIG. 3. As in Fig. 2 except that $f = 10^{-4}$ s^{-1}.

$$\sqrt{1 + \frac{m^2f^2}{k^2N^2}}.$$

Furthermore, the group velocity reduction is inversely proportional to the vertical wavenumber. This correlation between the group speed and the vertical wavelength predicts that rotation retards the wave energy dispersion, especially by short waves, and thus confines the response.

Figure 3 shows results for $f = 10^{-4}$ s^{-1}, corresponding to about 40°N. The Coriolis acceleration, which has no effect on total kinetic energy, substantially reduces u (Fig. 3a) compared with $f = 0$. The far-field low-level inflow and upper-level outflow patterns are hardly affected. During adjustment toward geostrophic balance, the Coriolis turning generates v momentum. Rotation substantially strengthens subsidence in the near field, but weakens the far-field subsidence associated with the fast mode (Fig. 3b). Low-tropospheric ascent associated with the slow mode is reduced significantly.

Similarly, the pressure perturbation (Fig. 3c) is localized to the neighborhood of the heating, but the large horizontal pressure gradient does not enhance u. Rather, the pressure gradient is almost balanced by the Coriolis acceleration as a result of the strong v. These rotation-

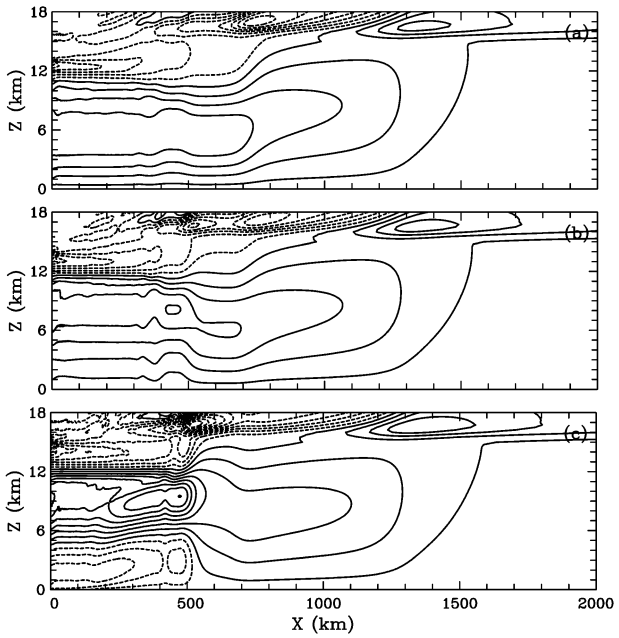

FIG. 4. Temperature perturbations at 8 h for $f = 0$. (a), (b), (c) Heating sources with $\gamma = 0$, 1/4, and 3/4, respectively. Contour interval is 0.5 K.

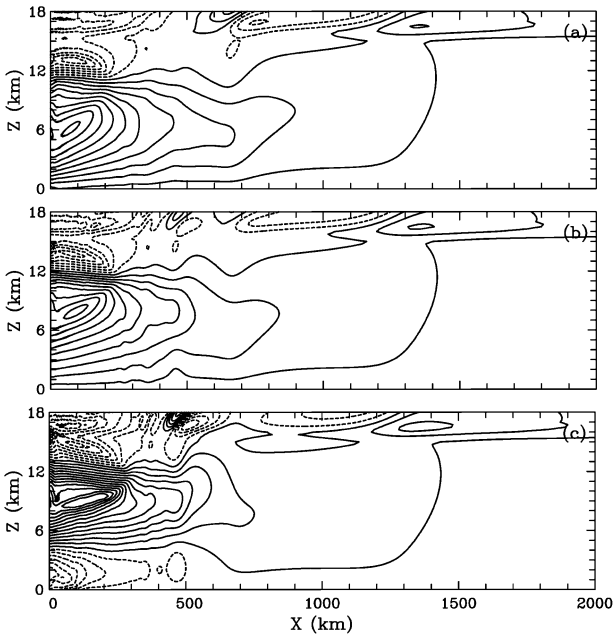

FIG. 5. As in Fig. 4 except that $f = 10^{-4}$ s^{-1}.

induced changes are closely associated with the buoyancy perturbations. Figure 3d illustrates that near-field middle-level warming is enhanced significantly although the far-field subsidence-induced warming and near-field low-level ascent-induced cooling are weakened. This is reflected in the vertical velocity field. The maximum midtropospheric warming is almost doubled by planetary rotation. In contrast, the far-field subsidence warming is more than halved. The maximum warming at 450 km is due to the slow mode in the rotation-free simulation and is more localized (at $x =$ 100 km) in the presence of rotation.

The horizontal phase speeds of the two gravest modes are little affected by planetary rotation compared to higher wavenumber waves, which have comparatively negligible effects. The difference is due to the dispersive nature of gravity waves in the vertical. Because the deeper modes travel faster, they move greater distances before rotation-induced effects act. In contrast, shallower modes are confined closer to the heat source.

In summary, planetary rotation generates v momentum at the expense of u momentum, confining the lateral extent of the compensating subsidence and adiabatic warming close to the heat source. This is consistent with linear arguments (Bretherton 1987).

c. Sensitivity to the heating profile

We investigated the sensitivity to the profiles defined by $\gamma = 0$, 1/4, and 3/4 illustrated in Fig. 1 for $f = 0$. Comparing Fig. 4 with Fig. 2d, the far-field temperature perturbation (beyond $x = 500$ km) is hardly affected, but near field is sensitive to the heating distribution. In particular, the midlevel warming gradually intensifies and the low-level warming decreases. As the stratiform-like heating increases, the low-level warming is eventually replaced by a marked cooling.

The physical interpretation is as follows. Because the fast gravity wave is primarily a response to deep heating, identical among the four heat sources, similar temperature perturbations beyond the leading edge of the slow wave are almost independent of the heating profile. In contrast, the slow wave is excited mainly by the stratiform heating and is increasingly important as the amplitude of the stratiform heating/cooling increases. It is responsible for the near-environment perturbations. Similar sensitivity occurs in the presence of planetary rotation (Fig. 5), and the rotational impact is qualitatively independent of heating profiles. Enhanced low-level lifting caused by the stratiform-like cooling suggests that convective systems with stratiform regions are conducive to a strong slow-wave mode favorable for initiating convection in the near environment. The response is approximately linear.

Figure 6 shows that rotation substantially enhances the warming over a near-field mesoscale region throughout the troposphere with a maximum in midtroposphere. Far-field warming is reduced. Additionally, the low-level adiabatic lifting and cooling are subdued, further stabilizing the near environment and decreasing the CAPE and possibly increasing the convective inhibition. It follows that rotation inhibits convection initiation in the near field but favors it in the far field by reducing heating-induced stabilization.

We now interpret the dry results in terms of a moist

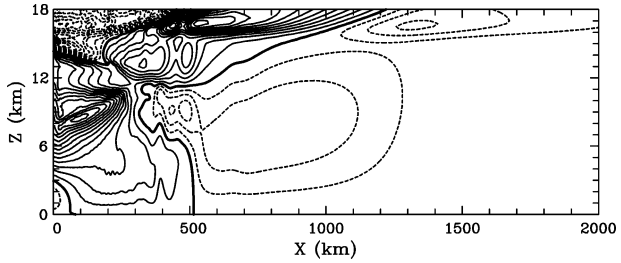

FIG. 6. Temperature difference at 8 h between simulations for $f = 10^{-4}$ s^{-1} and $f = 0$ (the former minus the latter). Heat source is defined by $\gamma = 1/2$ in both simulations. Contour interval 0.25 K, and thick lines are zero isolines.

atmosphere where, recall, two dominant gravity modes are excited by deep convective and stratiform-like heating. The subsidence warming is a maximum in midtroposphere, which decreases the convective available potential energy in a moist atmosphere. This is consistent with the long-held conception that compensating subsidence around convection suppresses the local onset of moist convection. On the other hand, the low-level lifting associated with the slow gravity wave mode increases CAPE and decreases the convective inhibition. This offsets midlevel stabilization in the adjacent environment and favors the initiation of convection. This explains the gregarious behavior of observed tropical cloud clusters (Mapes 1993). In a moist atmosphere, ascent and descent motions would affect the humidity of cloud environment as well as the adiabatic heating and cooling. Subsidence-enhanced drying increases the evaporation of cloud- and rain-water and decreases the precipitation efficiency. The equivalent potential temperature in the boundary layer, and therefore the CAPE, is decreased by the entrainment of overlying dry air and by unsaturated downdrafts. Enhanced entrainment in a drier environment further decreases CAPE. Accordingly, downward motions associated with the gravity wave response to thermal forcing will suppress convection through a warming-induced increase in static stability and drying.

Coriolis-confined subsidence results in stronger, localized warming and drying, and thus is harmful to development of further convection. In the far environment, on the other hand, rotation weakens the warming and drying and favors convection initiation. The region of enhanced warming progressively broadens but is nevertheless limited to the leading edge of the slow mode. For mesoscale convective systems having a typical lifetime of several hours, the confinement occurs on mesoscales.

The above argument suggests that convection should be more persistent, clustered, and gregarious in the Tropics than in higher latitudes. This hypothesis is now evaluated by performing multiday, large-domain simulations of precipitating cloud systems.

4. Multiscale clustering and convective organization

Two-dimensional cloud-resolving simulations are conducted with the same numerical model used for the dry simulations. Multiscale experiments require a large (4000 km $\times$ 24 km) domain. The horizontal and vertical grid intervals are 2 km and 0.3 km, respectively. The lower boundary represents a constant-temperature (302.5 K) ocean surface. Surface fluxes are parameterized by the Fairall et al. (1996) scheme. Microphysical processes are represented by a two-category warm-rain parameterization (Grabowski and Smolarkiewicz 1996) and ice parameterization (Grabowski 1999). Constant radiative cooling of 1.5 K day^{-1} is imposed below 12 km, decreasing linearly to zero at the model top.

The model was initialized with the average thermodynamic profile of the convectively active 19–26 December 1992 period of the Tropical Ocean Global Atmosphere Coupled Ocean–Atmosphere Response Experiment (TOGA COARE). Two sets of three 12-day numerical experiments were conducted, representative of the Tropics ($f = 0$), subtropics ($f = 0.5 \times 10^{-4}$ s^{-1}), and midlatitudes ($f = 10^{-4}$ s^{-1}). One set of experiments has a motionless mean state. In the other, a uniform easterly (6 m s^{-1}) is maintained by a Newtonion relaxation procedure.

Figure 7 shows the space–time distribution of the surface precipitation rate in the three simulations with motionless mean flow. In the Tropics, numerous convective systems persist for 12–24 h (Fig. 7a), significantly longer than in the subtropics (Fig. 7b) or in the midlatitudes (Fig. 7c). No convective system survives longer than 12 hours apart from early in the second day when planetary rotation is in operation. Midlatitude convection is the shortest lived. The inverted V shape signifies deep convection triggered by outflow from evaporatively driven downdrafts (density currents) as quantified by Liu and Moncrieff (2001). Clustering is marked in the Tropics but the convection becomes progressively homogeneous as f increases.

Figure 8 shows that the convective organization is more complex in constant easterly flow. A coherent pattern of active convection propagates eastward at $\sim$14 m s^{-1} in the tropical case, comparable to the phase speed of the slow mode in an easterly flow of 6 m s^{-1}. MCSs embedded within the cloudy region travel westward. This manifestation of convectively coupled gravity waves resembles the large-scale organization in the cloud-system simulation of Oouchi (1999) and Grabowski and Moncrieff (2001). It occurs for all three values of f but is most prominent in the Tropics. The decreasing spatial scale of the coherent convection as f increases is consistent with the smaller Rossby radius of deformation. Because the mean flow is relaxed to the initial profile, the convective response for different values of the Coriolis parameter is attributed to rotation-induced confinement and accumulation of subsidence-

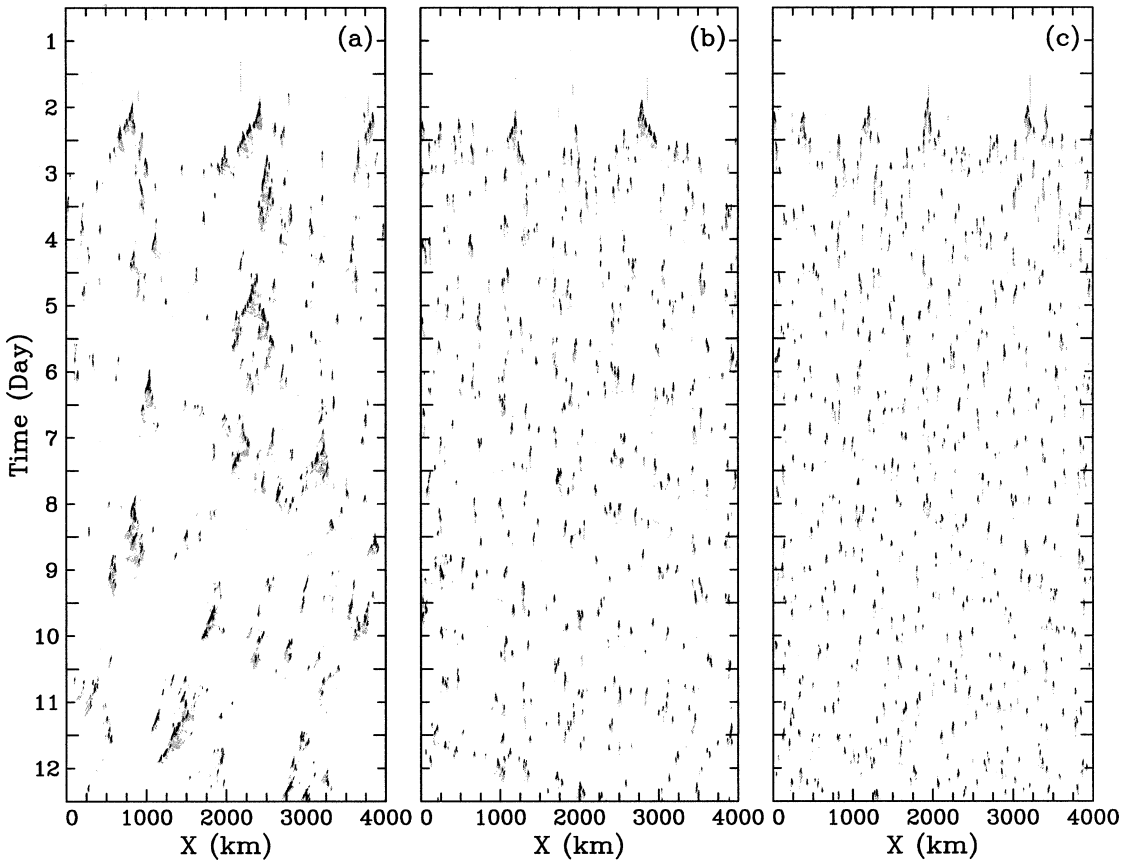

FIG. 7. Space–time distributions of the surface precipitation rate for simulations having a motionless initial state: (a) $f = 0$, (b) $f = 0.5 \times 10^{-4}$ s^{-1}, and (c) $f = 10^{-4}$ s^{-1}. The light and dark shading show precipitation rate larger than 0.1 and 10 mm h^{-1}, respectively.

induced warming and drying rather than to large-scale horizontal wind variability due to Coriolis turning. A convective envelope is also discernible in motionless mean flow (Fig. 7a) and travels at ~20 m s^{-1} (approximately the value of the second gravest mode).

The distributions of CAPE over a subdomain and a 4-day period in Fig. 9 exemplify the environmental modulations by convectively generated gravity waves. Note that the imposed radiative cooling and surface fluxes of sensible heat and moisture also modify the thermodynamic fields. However, this effect is compromised by the fact that the radiative forcing is time-independent and horizontally homogeneous and the effect of surface fluxes is relatively slower than the effect of gravity waves. Because CAPE is an integral quantity over a deep layer, its temporal and spatial variations largely represent the thermodynamic changes associated with the deep, fast-moving modes and the effects of higher wavenumber waves are mostly filtered out.

Three mesoscale clusters can be identified in the tropical case (Fig. 9a), initiated near 2500 km on day 5, 2200 km on day 7, and 3200 km on day 7. Figure 9b evinces the thermodynamic effects associated with these convective systems. As expected, the in-cloud and the previously convecting areas are substantially stabilized due to the evaporatively generated cold surface outflow. The most interesting feature is the region of high CAPE ahead of the active convection, presumably resulting from gravity waves. The upstream CAPE enhancement is also evident even for smaller-scale, less organized convection. In contrast, the short-lived convection in the midlatitude case (Fig. 9c) corresponds to strong localized stabilization (Fig. 9d) due to the rotational confinement. The striking difference between the two cases is consistent with the inference from the idealized dry simulations, but the detailed analyses and comparisons are complicated by the multiple, unsteady, and mobile heating sources in the cloud-resolving simulations.

5. Conclusions

The effects of gravity waves on the response of a uniformly stratified dry atmosphere to steady heating, representing latent heat release by precipitating convection, illustrate basic properties. Subsidence-induced warming, which accumulates with time, is confined by planetary rotation to the neighborhood of the heat source. In the far-field, subsidence warming is weak-

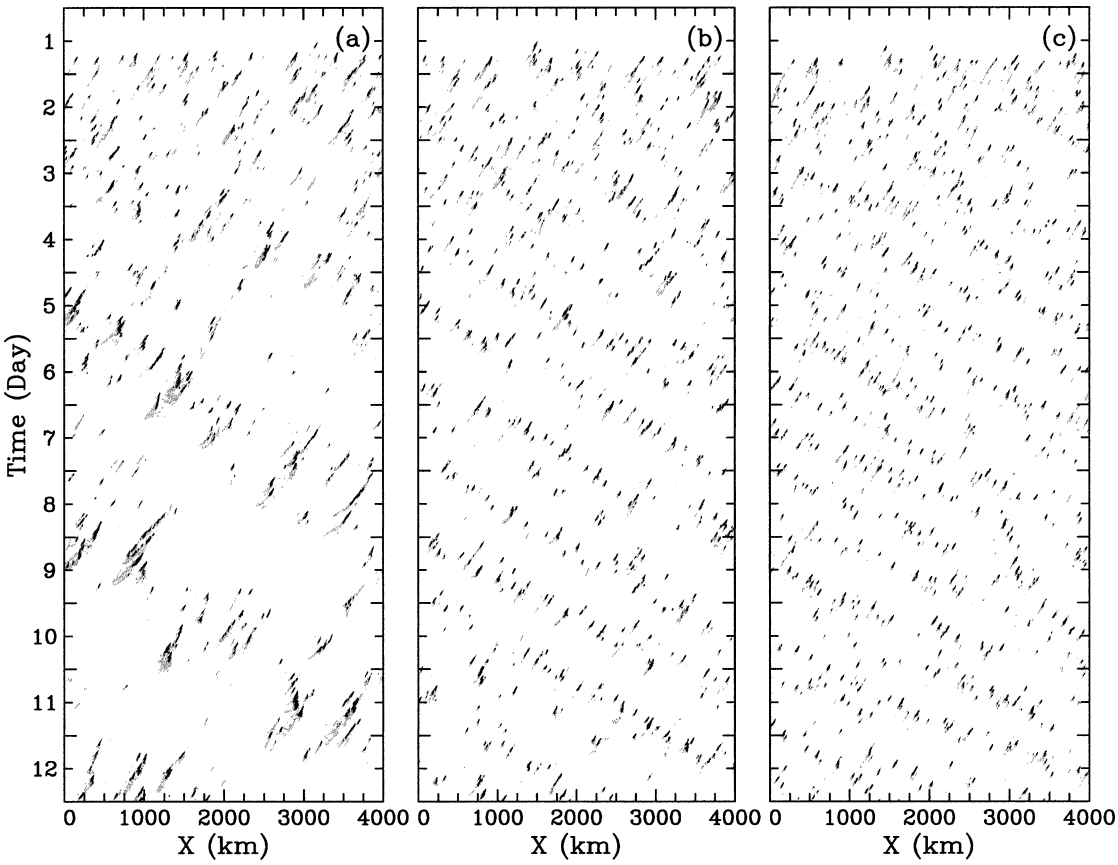

FIG. 8. As in Fig. 7 except that an easterly mean flow 6 m s^{-1} is maintained by Newtonian relaxation.

ened: planetary rotation enhances (lessens) the static stability in the near-environment vicinity (far environment) of vigorous deep convection.

In a moist atmosphere, the planetary-rotation confinement concentrates drying in the neighborhood of convective systems and reduces drying in the far field. The localization and accumulation of subsidence warming and drying is detrimental to convection in the near field because it decreases CAPE and increases the convective inhibition.

The vertical distribution of heating affects the amplitudes of the two gravest modes (for brevity called fast and slow waves). Because the fast wave is a response to deep heating, temperature and moisture perturbations beyond the leading edge of the slow wave are almost independent of the heating profile. On the other hand, the slow wave is excited by the stratiform heating. As the amplitude of the stratiform heating/cooling increases, its effect on the near environment becomes comparatively more important for all values of f. The enhanced low-level lifting implies that convective systems with stratiform regions are conducive to a strong slow-wave response and, therefore, to the initiation/maintenance of convection in the near environment.

Enhancement of CAPE in the near field by stratiform heating through slow-wave dynamics is reflected in the effect of cloud microphysics on latent heating (Grabowski 2003). Typically, ice physics generate more extensive stratiform regions and evaporative cooling than ice-free physics. This is consistent with the stratiform-heating response for $\gamma = 3/4$ that enhances the CAPE and promotes convection in the near field. Conversely, reduced warming and drying by planetary rotation favors convection in the far field. Rotation-modulated compensating subsidence (warming and drying) indicates that the low values of f in the Tropics will favor convective clustering. This quantifies the relationship between the gregarious properties of convection and convectively generated gravity waves (Mapes 1993).

This hypothesis is confirmed by multiday convection-resolving simulations. In a motionless mean state, the clustering of convection is strongest in the Tropics. Constant easterly mean flow reveals a three-scale organization of convection. Convectively coupled gravity waves propagate eastward as large-scale envelopes of precipitating convection. Embedded within these envelopes are westward-traveling MCSs that, in turn, contain westward-traveling deep convective cores. The hypothesis also provides an explanation for the latitudinal dependence of convective clustering reported in two-dimensional general circulation modeling on f planes

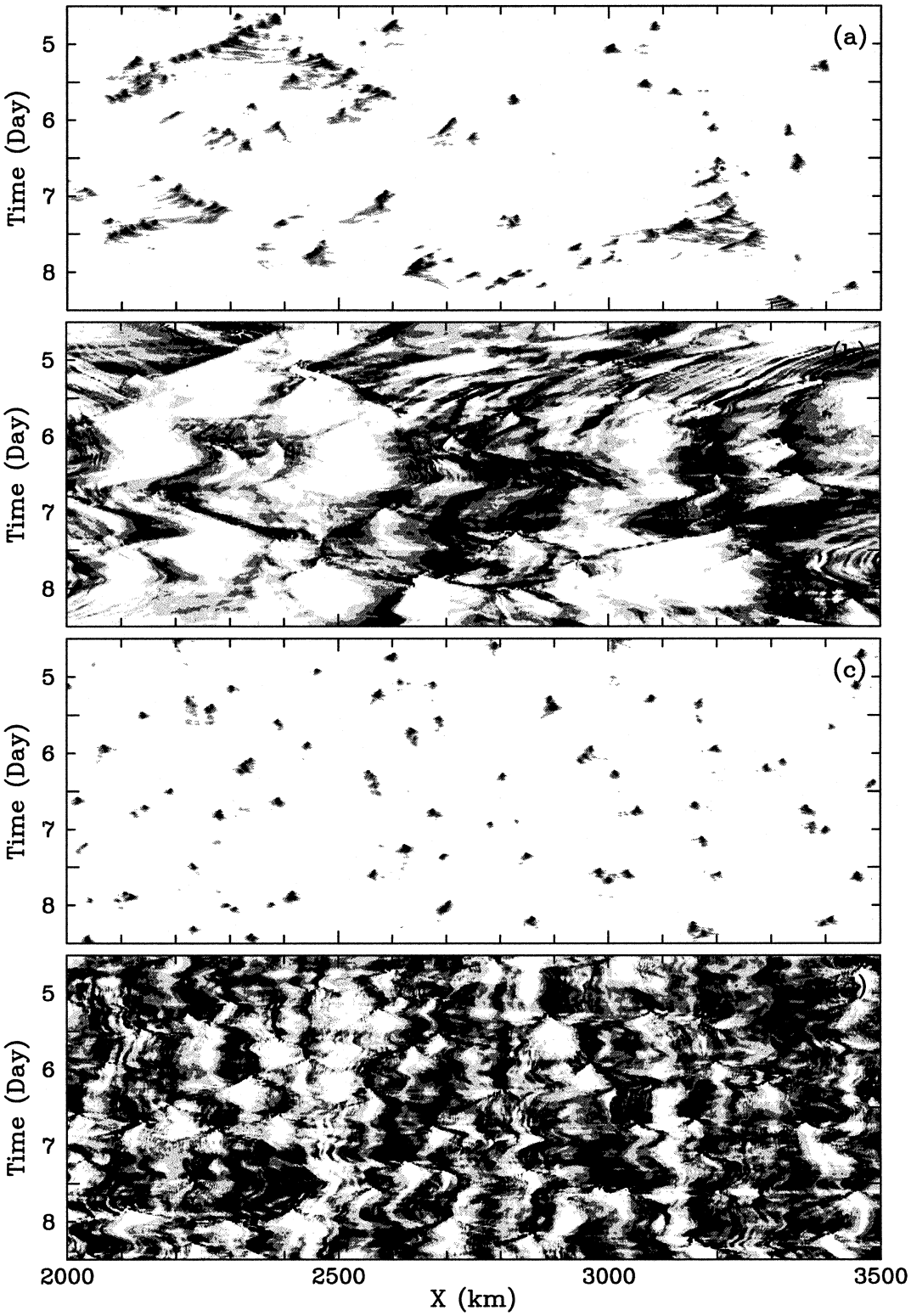

FIG. 9. Space–time distributions of the precipitation rate and CAPE for simulations having a motionless initial state. (a), (b) Precipitation and CAPE, respectively, in the tropical case; (c), (d) Precipitation and CAPE, respectively, in the midlatitude case. The light, moderate dark, and heavy dark shading represent values larger than (a), (c) 0.1, 1, and 10 mm h^{-1}, respectively, and (b), (d) 1, 1.5, and 2 kJ kg^{-1}, respectively.

(Chao and Lin 1994) and in explicit simulations on an equatorial β plane (Liu and Moncrieff 2004).

The importance of three gravest modes on CAPE and convective inhibition was stressed by Lane and Reeder (2001) for a single convective cell. In their case, the far-field CAPE was reduced by 15% and the near-field convective inhibition was reduced by 33%. Therefore, even a single unorganized convective cell can affect the environment sufficiently to promote clustering. In our case the two gravest modes had by far the largest amplitude. In addition, the second mode in Lane and Reeder (2001) produces negative displacements at low levels and positive displacements at upper levels, unlike the structure of vertical motions in the idealized simulations. The cause of these differences warrants further investigation.

The results in this study are subject to the limitation of the two-dimensional geometry. In three spatial dimensions, the amplitude of gravity waves decays away from the source but not in a two-dimensional framework. Accordingly, we expect that the convectively excited gravity waves would produce weaker environmental modifications in the real world. Also, one needs to be cautious when applying the modeling results to the real atmosphere. The conclusions drawn from the idealized simulations are valid in the absence of the large-scale forcing or in the weakly forced conditions and at time scales longer than the lifetime of an MCS. The real atmosphere is complicated by other influences, such as the vertical wind shear, strong forcing associated with frontal lifting, various synoptic systems, and mesoscale processes.

Acknowledgments. We are grateful to Todd Lane for helpful suggestions. We also would like to thank the anonymous reviewers for their constructive comments. The National Center for Atmospheric Research is sponsored by the National Science Foundation. This research was partly supported by the NASA TRMM Grant NAG5-7742.

REFERENCES

Bretherton, C. S., 1987: A theory for nonprecipitating convection between two parallel plates. Part I: Thermodynamics and ''linear'' solutions. *J. Atmos. Sci.,* **44,** 1809–1827.

——, 1988: Group velocity and the linear response of stratified fluids to internal heat or mass sources. *J. Atmos. Sci.,* **45,** 81–93.

——, and P. K. Smolarkiewicz, 1989: Gravity waves, compensating subsidence and detrainment around cumulus clouds. *J. Atmos. Sci.,* **46,** 740–759.

Chao, W. C., and S.-J. Lin, 1994: Tropical intraseasonal oscillation, super cloud clusters, and cumulus convection schemes. *J. Atmos. Sci.,* **51,** 1282–1297.

Clark, T. L., T. Hauf, and J. P. Kuettner, 1986: Convectively forced internal gravity waves: Results from two-dimensional numerical experiments. *Quart. J. Roy. Meteor. Soc.,* **112,** 899–925.

Fairall, C. W., E. F. Bradley, D. P. Rogers, J. B. Edson, and G. S. Young, 1996: Bulk parameterization of air–sea fluxes for Tropical Ocean-Global Atmosphere Coupled-Ocean Atmosphere Response Experiment. *J. Geophys. Res.,* **101,** 3747–3764.

Fovell, R., D. Durran, and J. R. Holton, 1992: Numerical simulations of convectively generated stratospheric gravity waves. *J. Atmos. Sci.,* **49,** 1427–1442.

Grabowski, W. W., 1999: A parameterization of cloud microphysics for long-term cloud-resolving modeling of tropical convection. *Atmos. Res.,* **52,** 17–41.

——, 2003: Impact of ice microphysics on multiscale organization of tropical convection in two-dimensional cloud-resolving simulations. *Quart. J. Roy. Meteor. Soc.,* **129,** 67–81.

——, and P. K. Smolarkiewicz, 1996: Two-time-level semi-Lagrangian modeling of precipitating clouds. *Mon. Wea. Rev.,* **124,** 487–497.

——, and M. W. Moncrieff, 2001: Large-scale organization of tropical convection in two-dimensional explicit numerical simulations. *Quart. J. Roy. Meteor. Soc.,* **127,** 445–468.

Kummerow, C., and Coauthors, 2001: The evolution of the Goddard Profiling Algorithm (GPROF) for rainfall estimation from passive microwave sensors. *J. Appl. Meteor.,* **40,** 1801–1820.

Lane, T. P., and M. J. Reeder, 2001: Convectively generated gravity waves and their effect on the cloud environment. *J. Atmos. Sci.,* **58,** 2427–2440.

——, ——, and T. L. Clark, 2001: Numerical modeling of gravity wave generation by deep tropical convection. *J. Atmos. Sci.,* **58,** 1249–1274.

Liu, C., and M. W. Moncrieff, 2001: Cumulus ensembles in shear: Implications for parameterization. *J. Atmos. Sci.,* **58,** 2832–2842.

——, and ——, 2004: Explicit simulations of the intertropical convergence zone. *J. Atmos. Sci.,* **61,** 458–473.

Mapes, B. E., 1993: Gregarious tropical convection. *J. Atmos. Sci.,* **50,** 2026–2037.

——, 1998: The large-scale part of tropical mesoscale convective system circulations: A linear vertical spectral band model. *J. Meteor. Soc. Japan,* **76,** 29–55.

Nicholls, M. E., R. A. Pielke, and W. R. Cotton, 1991: Thermally forced gravity waves in an atmosphere at rest. *J. Atmos. Sci.,* **48,** 1869–1884.

Oouchi, K., 1999: Hierarchical organization of super cloud cluster caused by WISHE, convectively induced gravity waves and cold pool. *J. Meteor. Soc. Japan,* **77,** 907–927.

Pandya, R., D. Durran, and C. Bretherton, 1993: Comments on ''Thermally forced gravity waves in an atmosphere at rest.'' *J. Atmos. Sci.,* **50,** 4097–4101.

Riehl, H., and J. S. Malkus, 1958: On the heat balance in the equatorial trough zone. *Geophysica,* **6,** 503–538.

Smolarkiewicz, P. K., and L. G. Margolin, 1997: On forward-in-time differencing for fluids: An Eulerian/semi-Lagrangian nonhydrostatic model for stratified flows. *Atmos. Ocean Spec.,* **35,** 127–152.

Tao, W.-K., and Coauthors, 2001: Retrieved vertical profiles of latent heat release using TRMM rainfall products for February 1998. *J. Appl. Meteor.,* **40,** 957–982.